Impact of the memory effect on the homogeneity of a Townsend Dielectric Barrier Discharge in air

A. Belinger[1], J. Haton[1], B. Lina[1], E. Sammier[1], S. Dap[1], L. Stafford[2], N. Naudé[1]

[1] *LAPLACE, Université de Toulouse, CNRS, INPT, UPS, Toulouse, France*
[2] *Département de Physique, Université de Montréal, Montréal, Québec, Canada*

Abstract: This work focuses on a diffuse Dielectric Barrier Discharge (DBD) obtained at atmospheric pressure in air. The discharge regime is analyzed with a short exposure time camera and electrical measurements. Contrary to other gases, the feature of this diffuse discharge is its relative inhomogeneity at a macroscopic scale, which is probably linked to the memory effect. Indeed, by modifying the dielectric material and using a segmented electrode, we discuss the origin of the memory effect (surface vs volume mechanisms).

Keywords: Dielectric Barrier Discharge, Townsend Discharge, Air, Memory effect.

1. Introduction

For many years, atmospheric pressure plasma technology has made significant progress and offers the opportunity to develop thin films deposition [1]. Among many devices, the Dielectric Barrier Discharge (DBD) device is often chosen to obtain a cold plasma at atmospheric pressure because dielectrics inserted between the two electrodes avoid the transition to the arc regime. It gives to DBDs their unique ability to generate cold discharges over large-scale surfaces. Hence DBDs are used to the existing Corona processes for continuous and large-scale production lines. Depending on the gas, electrical parameters and electrode configuration, the DBD can operate in the classical filamentary mode or in the homogeneous regime [2–4]. In the filamentary regime, discharge consists of very short lifetime (1-10 ns) filaments independent from each other [4,5] and randomly distributed. Therefore, the energy transferred to the surface is not uniform, representing a major drawback to the use of DBD in applications such as plasma coating or surface treatment. To obtain a dense and homogeneous coating, the DBD must preferably work in a diffuse regime. This regime is easily observed in noble gases or nitrogen but hardly in air [6]. However, in 2011, Osawa *et al.* presented for the first time a homogeneous discharge in air at low frequency (until 1 kHz) [7,8]. We present recently a diffuse discharge in air at 5 kHz with a power density of 0.5 W/cm^2 [9]. This value is close to the results reported in the literature for the first coating in nitrogen atmosphere [10,11]. This result paves the way for industrial application development in air at atmospheric pressure, like coating. However, the growth rate depends directly on the discharge power [12]. The development of surface treatment in air depends on the increase of the power in the diffuse regime and then on understanding the mechanisms leading to this regime.

At atmospheric pressure, seed electrons are required before the ignition to obtain a Townsend breakdown and then a diffuse discharge [6]. This phenomenon is called the memory effect because the source of the seed electrons results from the previous discharges. Its origin can come from gas or volume mechanisms. For example, the long lifetime metastable molecules $N_2(A^3\,\Sigma_u^+)$ observed in nitrogen is involved in the volume memory effect [6]. However, due to the oxidizing species, this metastable states cannot be involved in the memory effect in air [13]. Generally, surface mechanism is not self-sufficient. However, Golubovskii *et al.* [14] showed that the desorption of electrons from the surface could be sufficient to obtain a Townsend discharge.

To better understand the seed electrons production mechanisms in air, we investigate the role of the surfaces by changing the dielectric material and the role of the gas by using a segmented electrode. Before that, the first part of this work is dedicated to the characterization of the homogeneity of the diffuse discharge in air.

2. Materials and methods

The plane-to-plane DBD is placed in a closed vessel which is pumped down to 10^{-3} mbar before any experiment. It is then filled up to atmospheric pressure using synthetic air (Alphagaz 1 from Air Liquide). To renew the atmosphere, a gas flow is injected from one side of the discharge, keeping a constant pressure through regulating the pumping of the vessel. Finally, the discharge is ignited between two dielectrics. Each dielectric is covered by a square electrode (A_e=3 cm * 3 cm). Several dielectric materials were used in this work; all of them are made in alumina plates of 1 mm with a purity of 96% and a relative permittivity ε_r=9.6.

A sinusoidal power supply is used to power the DBD. A shunt resistor of 1000 Ω held the current measurement of the DBD. The DBD voltage (V_a) is measured by a high-voltage probe (Tektronix P6015A). Current and voltage measurements of the DBD are then recorded using a 1 GHz oscilloscope – 10 bits (Rohde and Schwarz – RTA 4004).

Short-exposure time photographs are taken with an intensified CCD camera (PI-MAX-3, Princeton Instruments) synchronized with the power supply and equipped with a visible lens (Nikkon NIKKOR 50 mm f/1.2). The camera is placed in the gas flow direction.

3. Diffuse discharge in air

The electrical characteristic of the discharge obtained in air at 2 kHz is presented in Fig. 1. The applied voltage V_a and the applied current I_a are directly measured, the gas gap voltage V_g and the discharge current I_d are calculated from an equivalent model of the discharge as presented in [9].

The waveforms clearly show the behavior of a diffuse discharge. The discharge current I_d has one large peak for each half-period. The gas gap voltage V_g is constant during the current peak as in a Townsend discharge.

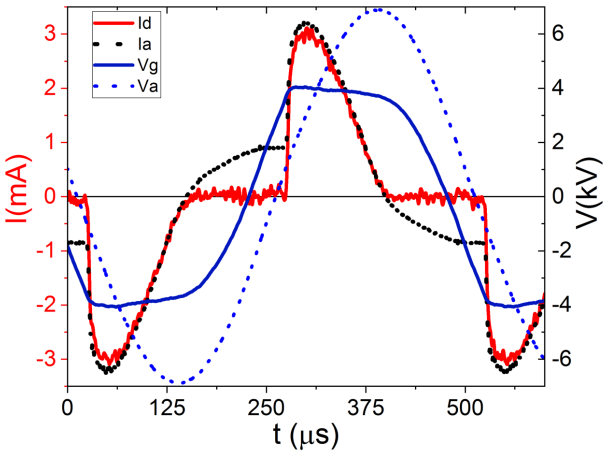

Fig. 1. Diffuse discharge in air at 2kHz

The diffuse character of the discharge is confirmed by short exposure time images presented in Fig. 2. These images are taken respectively on the positive and negative polarities with an exposure time equal to the half period. The bright region is always located on the anode side, as in a Townsend discharge. Therefore, we can conclude that the diffuse discharge observed in air is a Townsend discharge, as in nitrogen.

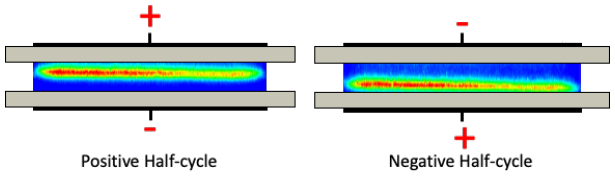

Fig. 2. Image of the discharge for both half-cycle. + and – indicated the cathode and the anode

The first Townsend coefficient can be calculated from the images in Fig. 2 by fitting the exponential growth of the light along the gas gap. The determined value is equal to $\alpha = 41$ cm^{-1}, then the electric field calculated from *Bolsig+* [15] with the IST-Lisbon database [16] equals 153 Td. Considering a constant electric field across the gap (typical of Townsend discharges), it is possible to calculate a gas gap voltage V_g=*3.8kV*, which is close to the gas voltage observed in Fig. 1. Then, the optical and electrical observations are consistent.

Looking closely at Fig. 2, the discharge is not homogeneous in its strictest definition. Indeed, the right part seems to be more luminous than the left part. To confirm the inhomogeneity of the discharge, a local measurement is needed. A segmented electrode consisting of 64 square segments (3.44 mm side length) helps obtaining the current mapping as it is presented in Fig. 3. This setup is described in [17].

As shown in Fig. 3, the current distribution is not strictly homogeneous. However, because the current intensity is distributed without any particular pattern, the flow seems to have no influence on the current distribution. Hence the inhomogeneity is probably not related to a volume mechanism.

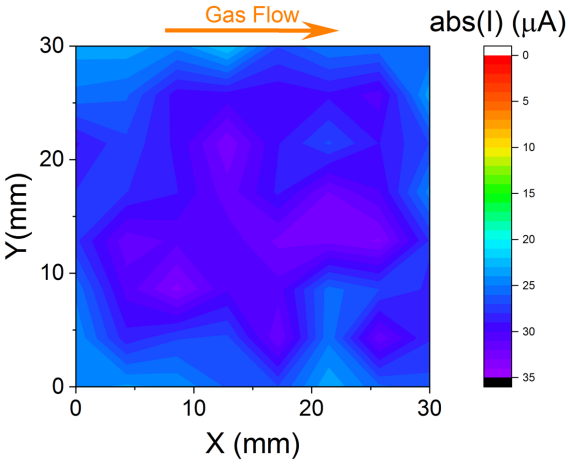

Fig. 3. Current distribution at the maximal value of the discharge current (V_a = 13.5kV$_{pp}$, f = 700 Hz)

To understand the origin of the inhomogeneity the discharge development is observed. Although, the segmented electrode cannot be used due to its acquisition system [17], the ICCD camera is well suited for nanosecond observation. To follow the time evolution of the discharge, the exposure time is reduced to 250 ns. Then to have the whole period at 2kHz, 2000 images are needed. As expected, the discharge produces light during the current peak. The inhomogeneity appears clearly at the ignition as shown in Fig. 4. The left part is more luminous than the right part.

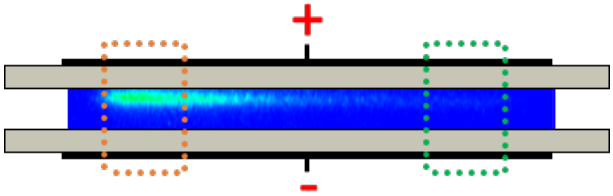

Fig. 4. Ignition of the discharge on the positive half-cycle (exposure time = 250 ns, 1000 ICCD accumulations)

A special focus on the time evolution of the electrode's left (orange) and right (green) zones enable to study the discharge development. For this purpose, each pixel's intensity in these zones is summed for each image. Normalized results are presented in Fig. 5. The same procedure is applied for both half-periods, and the absolute value of the discharge current is added for comparison (blue curve).

Whatever the half cycle, a delay of 2 µs exists between the discharge ignition of the right and the left zones. Then the electron avalanche is not uniform along the dielectric

surface. It systematically starts earlier on the left part of the discharge. Moreover, in "steady state" the light intensity emitted in the left part is 20 % higher than in the right part. At atmospheric pressure in air the light emission is dominated by the nitrogen Second Positive System (SPS) which is dominantly exited by direct electron impact from the ground state [18]. It suggests that the electron density in front of the anode is higher in the left part. During the discharge, more electrons are then stored on the dielectric surface in the left part of the electrode. When the polarity is reversed for the next half-period, the old anode becomes the new cathode. If a mechanism can easily release electrons from the dielectric surface (memory effect), the distribution of seed electrons along the dielectric is inhomogeneous. In this case, the seed electrons from the orange area can facilitate the breakdown, which occurs earlier, *i.e.* at a lower voltage for a sinusoidal excitation. As a virtuous circle, the discharge is consequently more intense in the left part. Then, this assumption could explain the inhomogeneity of the discharge.

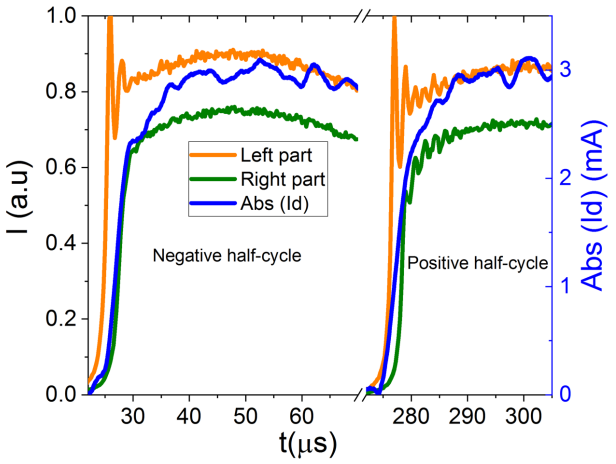

Fig. 5. Evolution of the light intensity on the left and on the right part of the discharge

The inhomogeneity of the discharge seems to be influenced by the storage of the electron on the dielectric surface. The ability to store the electron being related to the dielectric material, it is interesting to study the influence of the dielectric material on the Townsend discharge.

4. Impact of the dielectric material

A Comparison of the ability to obtain a Townsend discharge is realized for three alumina materials: COORSTEK, KYOCERA and KYOCERA TT (thermal treatment). Except the alumina material the experimental parameters are unchanged: same dielectric capacitance, same gas gap and same gas flow (1slm). A quantification of the memory effect is now needed to compare the material.

To obtain a diffuse discharge, the presence of seed electrons is mandatory, but it is also necessary to limit the ionization velocity *i.e.* the discharge current. With a sinusoidal excitation, the current magnitude is directly linked to the excitation frequency. For a given DBD device, the higher the seed electrons quantities, the higher the frequency where the discharge is diffuse. Because the dielectric capacitance is the same, the maximum frequency is used here as the image of the memory effect strength. Table 1 presents this maximum frequency for the three studied materials.

Table 1. Maximum frequency of Townsend discharge

Alumina Material	Maximum frequency
KYOCERA	4 kHz
KYOCERA TT	2.7 kHz
COORSTEK	1.1 kHz

Dielectric materials clearly influence the memory effect. Indeed, seed electron quantity should be more important for the KYOCERA alumina than for the COORSTEK alumina. It is interesting to compare this result to the charge storage ability of the dielectric. Thus, a potential probe system is used to quantify the electrical charging of the dielectric surface by the Townsend discharge by translating the material under the potential probe. Due to the time of the movement between the probe and the discharge cell, the surface potential measurement begins 1 s after the discharge. The time evolution of the maximum surface potential V_{suf} is presented in Fig. 6.

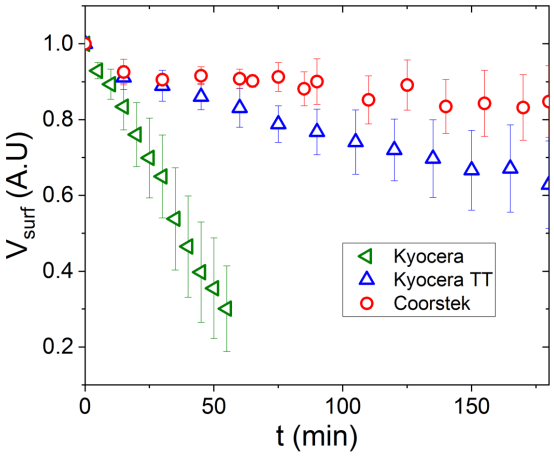

Fig. 6. Time evolution of the Surface Potential

The COORSTEK material stores the electric charges for the longest time whereas the surface potential decreases quickly for the KYOCERA. KYOCERA alumina plates release the electric charges easily compared to the other materials. Consequently, the quantity of seed electrons present in the gas gap could be more important with the KYOCERA. Hence it is possible to obtain diffuse discharge at a higher frequency for KYOCERA materials compared to the two others.

The ability to obtain a Townsend discharge in air seems to be related to the ability of the dielectric to release the electrons. Hence, the memory effect in air is certainly ruled by a surface mechanism. Among them, electron

desorption [14] is a good candidate, in agreement with our results. Moreover, this surface mechanism could cause the inhomogeneity of the discharge as previously discussed. However, a volume memory effect could also exist, this point must be checked.

5. Volume memory effect

In this part, an eight bands segmented electrode is used to probe the discharge current along the gas flow and thus, the gas residence time. The system is similar to the study of Tyl *et al.* [13]. Three bands are selected as shown in Fig. 7: the entrance and the exit correspond respectively to the entrance and the exit of the gas flow. The current growth appears first at the entrance, then in the middle and finally at the exit. Moreover, the gas voltage is higher at the exit compared to the entrance. Both results show that the memory effect is probably higher at the entrance compared to the exit of the DBD which is the opposite behaviour compared to the diffuse discharge obtained in the presence of a volume memory effect, *e.g.* in nitrogen [13]. It could even involve a counter-memory effect. The electronegativity of the oxygen which causes attachment of electrons and the subsequent formation of negative ions could also probably reduce the amount of seed electrons produced by the surface mechanism [19]. In any case, if a volume mechanism exists, it is weaker to counterbalance the surface memory effect.

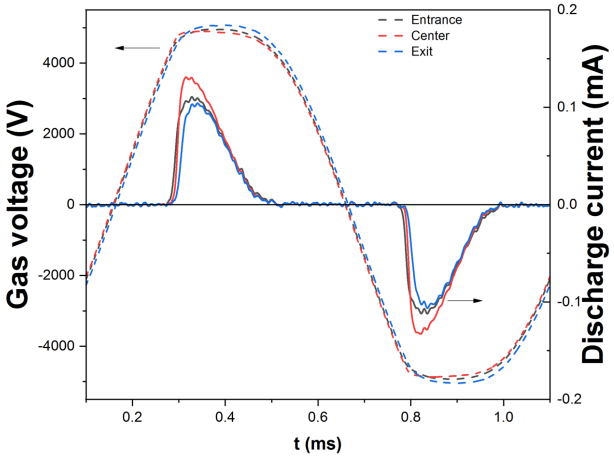

Fig. 7. Time evolution of the Gas gap voltage and the Discharge current at 3 positions of the electrode (f= 1kHz and V_a=15 kV_{pp}). Gas flow 1slm

6. Conclusion

The diffuse discharge obtained in air with a sinusoidal voltage work in the Townsend regime. This diffuse discharge is not fully homogeneous. This inhomogeneity is probably influenced by the production of seeds electron in specific regions of the dielectric surface. The dielectric material impacts the ability to obtain a Townsend discharge. Hence a surface mechanism is likely to be responsible for the seed electrons production and probably for the inhomogeneity of the diffuse discharge. This surface memory effect is clearly stronger than any hypothetical volume memory effect.

7. Acknowledgements

The authors would like to acknowledge financial support from Agence Nationale de la Recherche (DECAIR project: ANR-20-CE08-0014).

8. Reference

[1] F. Massines, C. Sarra-Bournet, F. Fanelli, N. Naudé, and N. Gherardi, Plasma Processes and Polymers **9**, 1041 (2012).

[2] U. Kogelschatz, Plasma Chemistry and Plasma Processing **23**, 1 (2003).

[3] P. J. Bruggeman, F. Iza, and R. Brandenburg, Plasma Sources Sci. Technol. **26**, 123002 (2017).

[4] R. Brandenburg, Plasma Sources Sci. Technol. **26**, 053001 (2017).

[5] P. Bruggeman and R. Brandenburg, J. Phys. D: Appl. Phys. **46**, 464001 (2013).

[6] F. Massines, N. Gherardi, N. Naudé, and P. Ségur, Eur. Phys. J. Appl. Phys. **47**, 22805 (2009).

[7] N. Osawa, H. Kaga, Y. Fukuda, S. Harada, Y. Yoshioka, and R. Hanaoka, Eur. Phys. J. Appl. Phys. **55**, 13802 (2011).

[8] N. Osawa and Y. Yoshioka, IEEE Trans. Plasma Sci. **40**, 2 (2012).

[9] A. Belinger, S. Dap, and N. Naudé, J. Phys. D: Appl. Phys. **55**, 465201 (2022).

[10] N. Gherardi, S. Martin, and F. Massines, Journal of Physics D: Applied Physics **33**, L104 (2000).

[11] F. Massines, N. Gherardi, A. Fornelli, and S. Martin, Surface and Coatings Technology **200**, 1855 (2005).

[12] F. Massines, C. Sarra-Bournet, F. Fanelli, N. Naudé, and N. Gherardi, Plasma Processes Polym. **9**, 1041 (2012).

[13] C. Tyl, X. Lin, M. C. Bouzidi, S. Dap, H. Caquineau, P. Ségur, N. Gherardi, and N. Naudé, J. Phys. D: Appl. Phys. **51**, 354001 (2018).

[14] Y. B. Golubovskii, V. A. Maiorov, J. Behnke, and J. F. Behnke, J. Phys. D: Appl. Phys. **35**, 751 (2002).

[15] G. J. M. Hagelaar and L. C. Pitchford, Plasma Sources Sci. Technol. **14**, 722 (2005).

[16] L. L. Alves, J. Phys.: Conf. Ser. **565**, 012007 (2014).

[17] C. Tyl, S. Martin, C. Combettes, G. Brillat, V. Bley, A. Belinger, S. Dap, R. Brandenburg, and N. Naudé, Review of Scientific Instruments **92**, 053552 (2021).

[18] K. V. Kozlov, H.-E. Wagner, R. Brandenburg, and P. Michel, J. Phys. D: Appl. Phys. **34**, 3164 (2001).

[19] S. Nemschokmichal, R. Tschiersch, H. Höft, R. Wild, M. Bogaczyk, M. M. Becker, D. Loffhagen, L. Stollenwerk, M. Kettlitz, R. Brandenburg, and J. Meichsner, Eur. Phys. J. D **72**, 89 (2018).